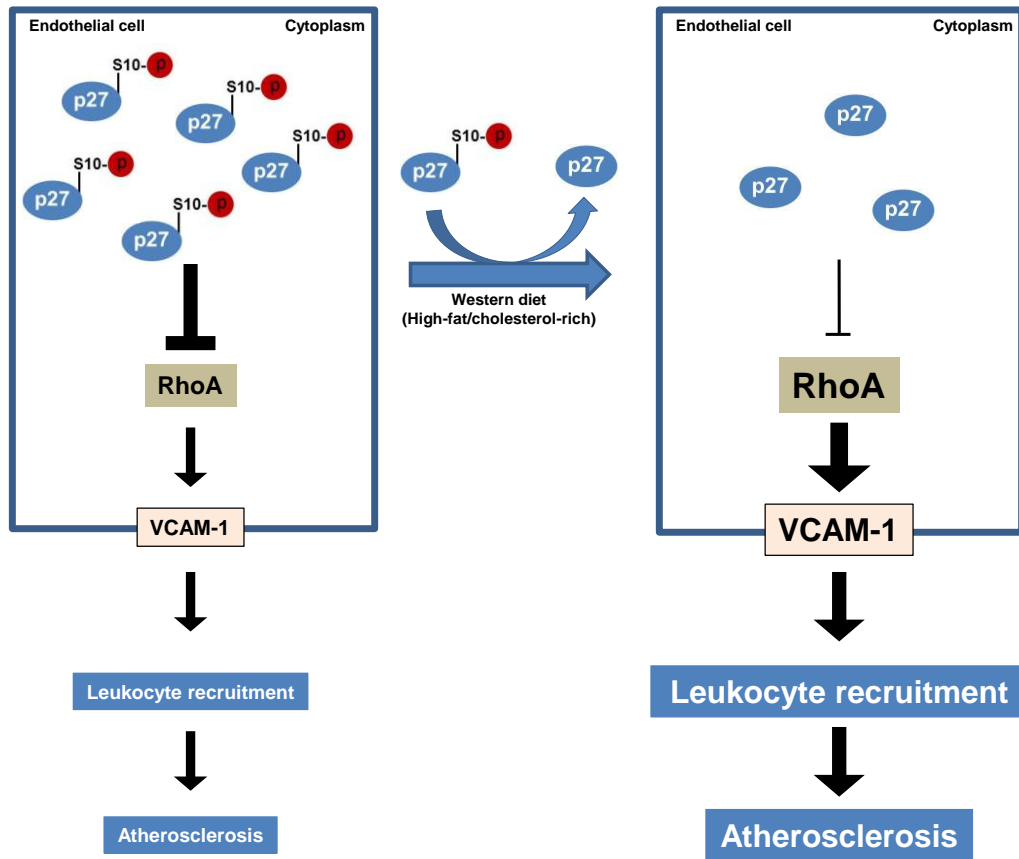


This is the peer reviewed version of the following article:

Molina-Sanchez P, Chevre R, Rius C, Fuster JJ, Andres V. Loss of p27 phosphorylation at Ser10 accelerates early atherogenesis by promoting leukocyte recruitment via RhoA/ROCK. *J Mol Cell Cardiol.* 2015;84:84-94.

which has been published in final form at: <https://doi.org/10.1016/j.yjmcc.2015.04.013>

### GRAFICAL ABSTRACT



## Highlights

- p27 is dephosphorylated at Ser10 in mouse aorta preceding plaque development
- Defective p27-phospho-S10 enhances adhesion molecule expression in aorta and endothelial cells
- Defective p27-phospho-S10 promotes leukocyte recruitment and early atherosclerosis
- RhoA/ROCK mediates the pro-atherogenic effects of defective p27-phospho-S10

**Loss of p27 phosphorylation at Ser10 accelerates early atherogenesis by promoting leukocyte recruitment via RhoA/ROCK**

Molina-Sánchez P.<sup>\*</sup>, Chèvre R.<sup>\*</sup>, Rius C., Fuster J.J.<sup>†</sup>, and Andrés V.<sup>‡</sup>

Laboratory of Molecular and Genetic Cardiovascular Pathophysiology, Centro Nacional de Investigaciones Cardiovasculares (CNIC), Madrid, Spain

\* Authors with equal contribution

† Current address: Whitaker Cardiovascular Institute, Boston University School of Medicine, Boston, US

‡ Corresponding author:

Laboratory of Molecular and Genetic Cardiovascular Pathophysiology  
CNIC

Melchor Fernández Almagro 3, 28029 Madrid (Spain)

Phone: +34-91 453 12 00 (Ext. 1502)

Fax: +34-91 453 12 65

E-mail: vandres@cnic.es

## Abbreviations

**apoE<sup>-/-</sup>**: apolipoprotein E-null; **apoE<sup>-/-</sup>p27Ser10Ala**: apolipoprotein E-null p27 Serine-10-Alanine; **BM**: Bone marrow; **CKI**: Cyclin-dependent Kinase Inhibitor; **DMEM**: Dulbecco's Modified Eagle Medium; **EC(s)**: Endothelial cell(s); **ECGS**: Endothelial Cell Growth Supplement; **EDTA**: Ethylenediaminetetraacetic acid; **ERM**: Ezrin/Radixin/Moesin; **E-Sel**: E-Selectin; **FBS**: Fetal Bovine Serum; **GFP**: Green Fluorescent Protein; **HBSS**: Hank's Balanced Salt Solution; **HFD**: High Fat Diet; **HRP**: Horseradish peroxidase; **ICAM-1**: Intercellular adhesion molecule-1; **IV**: Intravenous; **L-Sel**: L-Selectin; **mAECs**: Mouse aorta endothelial cells; **Mafia**: Macrophage Fas-Induced Apoptosis; **P-Sel**: P-Selectin; **p27**: p27<sup>Kip1</sup>; **p27-phospho-Ser-10**: p27 phosphorylation at Serine 10; **p27Ser10Ala**: p27 Serine-10-Alanine; **PBS**: Phosphate Buffered Saline; **PCR**: Polymerase Chain Reaction; **qPCR**: quantitative real-time PCR; **ROCK**: Rho-associated coiled-coil containing protein kinase; **Ser10**: Serine 10; **SDS**: Sodium Dodecyl Sulfate; **TNF $\alpha$** : Tumor Necrosis Factor- $\alpha$ ; **VCAM-1**: Vascular Cell Adhesion Molecule-1.

## Highlights

- p27 undergoes rapid dephosphorylation at serine 10 (Ser10) in aorta of fat-fed apoE<sup>-/-</sup> preceding development of macroscopically-visible lesions.
- Defective p27-phospho-Ser10 enhances the expression of adhesion molecules in aorta of apoE<sup>-/-</sup> mice and primary endothelial cell cultures.
- Defective p27-phospho-Ser10 augments endothelial-leukocyte interactions, leukocyte recruitment and early atherosclerosis development.
- Pharmacological inhibition of RhoA/ROCK blunts the pro-atherogenic effects of defective p27-phospho-Ser10.

## Keywords

atherosclerosis; endothelial cell; leukocyte recruitment; p27; RhoA

## Abstract

Reduced phosphorylation of the tumor suppressor p27<sup>Kip1</sup> (p27) at serine 10 (Ser10) is a hallmark of advanced human and mouse atherosclerosis. Apolipoprotein E-null mice defective for this posttranslational modification (apoE<sup>-/-</sup>p27Ser10Ala) exhibited increased atherosclerosis burden at late disease states. Here, we investigated the regulation of p27 phosphorylation in Ser10 at the very initial stages of atherosclerosis and its impact on endothelial-leukocyte interaction and early plaque formation. Hypercholesterolemia in fat-fed apoE<sup>-/-</sup> mice is associated with a rapid downregulation of p27-phospho-Ser10 in primary endothelial cells (ECs) and in aorta prior to the development of macroscopically-visible lesions. We find that lack of p27 phosphorylation at Ser10 enhances the expression of adhesion molecules in aorta of apoE<sup>-/-</sup> mice and ECs, and augments endothelial-leukocyte interactions and leukocyte recruitment *in vivo*. These effects correlated with increased RhoA/Rho-associated coiled-coil containing protein kinase (ROCK) signaling in ECs, and inhibition of this pathway with fasudil reduced leukocyte-EC interactions to control levels in the microvasculature of p27Ser10Ala mice. Moreover, apoE<sup>-/-</sup>p27Ser10Ala mice displayed increased leukocyte recruitment and homing to atherosusceptible arteries and augmented early plaque development, which could be blunted with fasudil. In conclusion, our studies demonstrate a very rapid reduction in p27-phospho-Ser10 levels at the onset of atherogenesis, which contributes to early plaque build-up through RhoA/ROCK-induced integrin expression in ECs and enhanced leukocyte recruitment.

## Introduction

Atherosclerosis and associated ischemic events are the leading cause of morbidity and mortality in Western societies and are predicted to soon become the leading health problem worldwide [1]. Several cardiovascular risk factors have been identified (dyslipidemia, hypertension, diabetes, smoking, aging, sedentary life style, etc.), which promote a chronic inflammatory state that leads to dysfunction of the endothelial cell (EC) monolayer lining the inner arterial surface [2]. One of the earliest manifestations of atherosclerosis is the expression of adhesion molecules by ECs, which triggers the recruitment of circulating leukocytes that normally do not interact with the 'healthy' vessel wall [3-9]. Leukocytes are considered important mediators of all phases of atherosclerosis, from the initiation and progression of asymptomatic lesions to the establishment of complex vulnerable plaques that can rupture and provoke acute ischemic events. Luminal recruitment appears to be the central route of leukocyte infiltration in the subendothelial space during early atherosclerosis since at these stages no *vasa vasora* can be detected, contrary to their reported abundance in late-stage atheromata [10]. Leukocytes roll and adhere to the endothelium to finally extravasate, and monocytes (the predominant leukocyte subset recruited in the damaged vessel wall) differentiate into macrophages that critically contribute to plaque development by secreting an array of inflammatory mediators [3-9].

Studies in animals and humans have identified excessive neointimal cell proliferation as a characteristic of atherosclerosis; consequently, regulation of hyperplastic growth of neointimal cells by tumor suppressors has emerged as a prominent mechanism regulating plaque development [11]. The oncosuppressor p27<sup>Kip1</sup> (p27) is a cyclin-dependent kinase inhibitor (CKI) that attenuates the proliferation of both vascular smooth muscle cells and macrophages, and also neointimal thickening in animal models of vasculoproliferative disease [11-16]. Interestingly, a micro-RNA-based strategy has been recently developed to selectively inhibit vascular smooth muscle cell hyperplasia while preserving EC proliferation and function, which attenuates restenosis post-angioplasty but allows complete reendothelialization [17].

Compelling evidence has emerged supporting a role for p27 beyond cell cycle control, including modulation of actin cytoskeleton, cell motility, and gene transcription [18-22]. A number of important functional aspects of p27 are regulated through its phosphorylation status [23-31]. We recently reported that sparse phosphorylation of p27 at serine 10 (p27-phospho-Ser10), the most common post-translational modification of p27 [23], is a hallmark of mouse and human atherosclerosis [32]. Moreover, apolipoprotein E-null mice defective for this post-translational modification (apoE<sup>-/-</sup>p27Ser10Ala) did not show alterations in neointimal cell proliferation, yet they had an increased atherosclerosis burden at advanced disease states, at least in part due to increased macrophage foam cell formation [32].

Since p27-phospho-Ser10 is involved in neointimal thickening by modulating proliferation-independent processes, we hypothesized that it could also promote EC dysregulation, which is thought to initiate and sustain atherosclerosis development [2, 5-7]. To address this issue, we have used complementary approaches with primary ECs and genetically-engineered mice. Our results demonstrate that loss of p27-phospho-Ser10 occurs rapidly in fat-fed apoE<sup>-/-</sup> mice and promotes VCAM-1 expression in ECs and leukocyte adhesion *in vivo*. Further, this defect also stimulates the formation of incipient atherosclerotic lesions through activation of the RhoA/Rho-associated coiled-coil containing protein kinase (ROCK) pathway.

## Material and methods

**Mice and diets.** apoE<sup>-/-</sup>p27Ser10Ala mice were generated by crossing nonphosphorylatable p27Ser10Ala knock-in mice [30] with apoE<sup>-/-</sup> mice (The Jackson laboratory, Madison, WI). Macrophage Fas-Induced Apoptosis (Mafia)-apoE<sup>-/-</sup> mice [3] were generated by crossing Mafia transgenic mice [33] (which express GFP in the myeloid lineage) with apoE<sup>-/-</sup> mice. Mafia apoE<sup>-/-</sup>p27Ser10Ala mice were generated by crossing Mafia-apoE<sup>-/-</sup> mice with apoE<sup>-/-</sup>p27Ser10Ala mice. All mice were on C57BL/6 background. Mice were maintained on a low-fat standard diet (2.8% fat; Panlab, Barcelona, Spain). For studies of diet-induced atherosclerosis, mice were placed on atherogenic high-fat diet (HFD) (10.8% total fat, 0.75% cholesterol, S4892-E010, Ssniff, Germany) for the indicated periods of time. In vivo studies were performed with 3-month-old mice. Care of animals was in accordance with institutional guidelines and regulations.

**Blood and serum collection and cholesterol analysis.** Mouse blood was extracted by submandibular puncture as described [34]. To obtain serum, 100 µl of blood was collected in polypropylene tubes, the blood was allowed to clot by leaving it undisturbed at room temperature for 30 minutes, and the clot was removed by centrifuging at 2000 x g for 15 minutes at 4°C. The serum was recovered and stored at -80°C until analyzed. Total and free cholesterol levels were measured using the automated analyzer Dimension RxL Max Clinical System (Siemens) in serum from mice which were starved overnight.

**Mouse anesthesia and euthanasia.** For intravital microscopy experiments (see below), mice were anesthetized with a mixture of ketamine and medetomidine (50 mg/kg and 0.5 mg/kg, respectively; intraperitoneal injection). Mice were euthanized by carbon dioxide inhalation.

**Isolation and culture of mouse aorta endothelial cells (mAECs).** mAECs from p27Ser10Ala mice and wild-type counterparts (both on C57BL/6 background) were isolated as described [35]. Briefly, 8 mice (8 weeks of age) were culled and aortas were rapidly harvested. After removing adipose tissue and adventitia layer, aortas were cut into 1 mm rings. Aortic rings were placed in gelatin (0.5 %) pre-coated plates and incubated in mAEC medium: DMEM:F12 (Lonza) containing 1% of penicillin/streptomycin, L-glutamine, 10 mM Hepes, Fungizone, 10% fetal bovine serum (FBS), 0.1 mg/ml of heparin (Sigma-Aldrich) and 50 µg/ml of endothelial cell growth supplement (ECGS, BD). After 7-12 days, mAECs were selected with CD102 antibody (Purified Rat Anti-Mouse CD102-ICAM-2 Monoclonal Antibody, BD Pharmingen) and with a secondary antibody linked to magnetic beads (Dynabeads Sheep anti-Rat IgG, Invitrogen) using a magnetic platform (DynaMag-15 Magnet, Life Technologies). These cells (passage 0) were expanded in gelatin-coated plates containing mAEC medium. All cells used for assays were between passages 4 and 7.

**Isolation of bone marrow (BM) cells.** BM cells were harvested from apoE<sup>-/-</sup>, apoE<sup>-/-</sup>p27Ser10Ala and Mafia-apoE<sup>-/-</sup> mice as described [36]. Briefly, femurs and tibiae were obtained from mice after carefully removing the surrounding skeletal muscle and fat tissue. Both ends of each bone were trimmed to expose the interior and the BM was flushed with Hank's Balanced Salt Solution (HBSS) containing 2 mM EDTA using a 1-ml insulin syringe with a 27G needle. The collected BM was disaggregated by pipetting and red blood cells were eliminated by 5 minutes incubation with cold lysis buffer (KH<sub>4</sub>Cl 0.15 M, KHCO<sub>3</sub> 0.01 M, EDTA.N2 0.01 M, pH 7.4). After washing with PBS, BM nucleated cells were kept on ice until used.

**Leukocyte adhesion in cremasteric vessels.** Mice were anesthetized and the cremaster muscle was dissected free of surrounding tissues and exteriorized onto an optical clear viewing pedestal. The muscle was cut longitudinally with a cautery and held extended at the corners of



the exposed tissue using surgical suture. To maintain the correct temperature and physiological conditions, the muscle was perfused continuously with warmed Tyrode's buffer. Four hours before surgery, animals were injected with 100  $\mu$ l of TNF $\alpha$  (0.5  $\mu$ g in 0.3 ml saline) to promote leukocyte-endothelial cell interactions. The cremasteric microcirculation was then observed using a Leica DM6000-FS intravital microscopy with an Apo 40x NA 1.0 water-immersion objective equipped with a DFC350-FX camera. LAS-AF software was employed for acquisition and image processing. Five randomly-selected arterioles were analyzed per mouse, and leukocyte adhesion was measured in 150- $\mu$ m vessel segments for 5 min. When indicated, IgG isotype control (AB-108-C, R&D Systems) or polyclonal anti-VCAM-1 antibodies (sc-1504, Santa Cruz Biotechnology) were injected intravenously prior to intravital microscopy (100  $\mu$ g/mouse).

**Intravital imaging of carotid artery and rolling.** Mice were anesthetized, the neck was shaved, and animals were immobilized in decubitus position. The right carotid artery was exposed and carefully dissected from the surrounding tissues [37]. to perform intravital imaging as described [3]. In brief, sutures were used to maintain the salivary gland and adjacent muscles away from the artery, and the right vague nerve was carefully separated from the artery. Throughout the procedure, warm saline was applied to the tissues. The carotid artery was stabilized and placed under the water-dipping objective of an epifluorescence microscope with constant perfusion with warm saline buffer. Images were captured with an Apo 63x NA 0.9 water-immersion objective in cy3 channel. For analysis, luminal cells of the carotid artery were labeled by intravenous (IV) injection of 50  $\mu$ g of rhodamine 6G (Sigma), and the number of rolling cells was determined by counting the number of rhodamine-positive leukocytes crossing an imaginary line perpendicular to the vessel during at least 30 seconds. Several fields (typically 3-4) were imaged from the carotid artery, and each data point represents one field. Although the appearance of plaques in the carotid artery is heterogeneous, for visualization we chose areas from the carotid bifurcation, which is prone to plaque development. Data were normalized to the number of rolling cells per 1000 frames.

**In vivo leukocyte homing.** To study leukocyte homing into the aorta, apoE<sup>-/-</sup>p27Ser10Ala mice and apoE<sup>-/-</sup> counterparts were injected twice for two days (IV) with five million nucleated BM cells (in a 200  $\mu$ L volume) from Mafia-apoE<sup>-/-</sup> mice, to allow detection of GFP-positive myeloid leukocytes (e.g. neutrophils and monocytes). After 48 hours, mice were killed, the aortic tissue was perfused *in situ* with PBS, harvested and immediately frozen. GFP expression in aortas was analyzed by quantitative real-time PCR.

**Atherosclerosis studies.** For quantification of atherosclerosis burden of aortic sinus, mice were sacrificed and the heart was harvested after *in situ* perfusion with PBS. Hearts were fixed overnight with 4% paraformaldehyde/PBS at 4°C. An operator blinded to genotype quantified the extent of atherosclerosis by computer-assisted morphometric analysis (ImageJ, National Institutes of Health) of hematoxylin/eosin-stained cross-sections of heart tissue, as described [38].

For quantification of infiltrated myeloid cells, Mafia-apoE<sup>-/-</sup>p27Ser10Ala mice and Mafia-apoE<sup>-/-</sup> counterparts were used, allowing the detection of GFP-positive myeloid cells (e.g. neutrophils, monocytes and macrophages). Mice were killed, the aortic tissue was perfused carefully *in situ* with PBS, harvested and immediately frozen. VCAM-1 and GFP expression was by quantitative real-time PCR (qPCR).

Macrophage detection in atheromata of aortic sinus was performed by F4/80 immunostaining. After deparaffinization, antigen retrieval and blocking of non-specific interactions (5% horse serum in PBS, 45 minutes), histological sections were incubated overnight at 4°C with anti-F4/80-Alexa Fluor 488 antibody (1/500, MCA497A488-AbD, Serotec). Cell nuclei were stained with DAPI (Invitrogen). Slides were mounted with Slow-Fade Gold Antifade reagent (S36936,

Invitrogen) and images were acquired on a Leica TCS/SP2 confocal microscope with a 40X oil immersion objective.

**Fasudil administration.** Animals were treated orally with a dose of 40 mg/kg/day of fasudil dissolved in drinking water. In the leukocyte-adhesion experiments in cremasteric arterioles and in the leukocyte homing assay in aorta, fasudil was administered daily, starting 4 days prior to surgery or sacrifice, respectively. For atherosclerosis studies, fasudil treatment started 4 days before putting mice on HFD and continued for 28 days.

**Gene expression analysis by quantitative real-time PCR (qPCR).** RNA from mouse aortic tissue or mAECs was obtained using TRIzol Reagent (Invitrogen). RNA (0.5-1µg) was retrotranscribed and amplified, respectively, with Superscript III First Strand Synthesis Supermix (Invitrogen) and Power Syber Green PCR Master Mix (Applied Biosystems). The following primers (Forward: Fw; Reverse: Rv) were used (5'→3' sequences):

<b>Selp_Fw</b>	GGTATCCGAAAGATCAACAATAAGTG
<b>Selp_Rv</b>	GTTACTCTTGATGTAGATCTCCACACA
<b>Sell_Fw</b>	AAACGAAAGGCAGCTCTCTG
<b>Sell_Rv</b>	CCCGTAATACCCTGCATCAC
<b>Icam1_Fw</b>	GGACCACGGAGCCAATTTTC
<b>Icam1_Rv</b>	CTCGGAGACATTAGAGAACAATGC
<b>Vcam1_Fw</b>	GACCTGTTCCAGCGAGGGTCTA
<b>Vcam1_Rv</b>	CTTCCATCCTCATAGCAATTAAGGTG
<b>E-GFP_Fw</b>	CCAGGAGCGCACCATCTTCTT
<b>E-GFP_Rv</b>	GTAGTGGTTGTCGGGCAGCAG
<b>Gapdh_Fw</b>	TGTGTCCGTCGTGGATCTGA
<b>Gapdh_Rv</b>	CCTGCTTCACCACCTTCTTGAT
<b>Hprt1_Fw</b>	CCTAAGATGAGCGCAAGTTGAA
<b>Hprt1_Rv</b>	CCACAGGACTAGAACACCTGCTAA
<b>36b4_Fw</b>	ACTGGTCTAGGACCCGAGAAG
<b>36b4_Rv</b>	TCCCACCTTGTCTCCAGTCT

Reactions were run on an ABI Prism 7500 Fast thermal cycler and results were analyzed with SDS 2.3 software (Applied Biosystems). Gene expression in both genotypes was normalized to the expression of the housekeeping genes *Hprt1*, *36b4* and *Gapdh* using Qbase software (Biogazelle).

**Western blot analysis.** Proteins from cultured mAECs and mouse aorta were extracted in an ice-cold lysis buffer containing 50 mM Tris-Cl, pH 7.2, 1% (w/v) Triton X-100, 0.1% (w/v) SDS, 500 mM NaCl and 10 mM MgCl<sub>2</sub>, supplemented with phosphatase and protease inhibitors (Roche). Polyacrylamide gel-electrophoresis and western blot analysis of whole cell extracts prepared in lysis buffer were performed as reported[39] and detection of proteins was carried out with the following antibodies: anti-p27 (610242) from BD Transduction Laboratories; anti- $\alpha$ -tubulin (sc-8035), anti- $\alpha$ -actin (sc-32251), anti- $\beta$ -actin (sc-130657), and anti-VCAM-1(sc-1504) from Santa Cruz Biotechnology; anti-ERM (3142) and anti-phospho-ERM (3149) from Cell Signaling Technology; anti-mCD54 ICAM (BE0020-1) and anti-CD62P P-selectin (clone RB40.34) from BioXcell and anti-p27-phospho-S10 (ab62364) from Abcam. HRP-conjugated secondary antibodies were from Santa Cruz Biotechnology. Immunocomplexes were detected with Luminata Forte Western HRP substrate (Millipore).

For the preparation of cytoplasmic lysates, mAECs were incubated for 15 minutes in ice-cold buffer containing 50 mM Tris-HCl (pH 7.5), 0.5% Triton X-100, 137.5 mM NaCl, 10% Glycerol, 1mM sodium vanadate, 50 mM sodium fluoride, 10 mM sodium pyrophosphate, 5 mM EDTA, and protease inhibitors (1mM PMSF, 10 ug/ml aprotinin, 10 ug/ml leupeptin). Lysates were centrifuged at 3000 rpm for 5 minutes, and the supernatant was stored at -80°C until western blot analysis.

**Flow cytometry analysis.** White blood cells were stained for Mac-1 (CD11b-APC (M1/70), TOMBO Biosciences), VLA-4 (CD49d-biotin (PS/2)/Streptavidin-APC, in-house and eBioscience, respectively), L-Selectin, and PSGL1 (CD62L-APC (MEL-14) and PSGL1-PE (2PH1), respectively, both from BD Biosciences). Mafia-p27Ser10Ala apoE<sup>-/-</sup> mice and Mafia-apoE<sup>-/-</sup> counterparts were used to discriminate GFP+ myeloid cells and GFP- lymphocytes. The anti-Ly6G antibody (clone 1A8, BioXcell) was used to discriminate GFP+ Ly6G+ neutrophils and GFP+ Ly6G- monocytes. The anti-Ly-6G antibody was labeled using DyLight 405 Antibody Labeling Kit (ThermoScientific). Cytometric analyses were performed using a FACS Canto flow cytometer equipped with DIVA software (BD Biosciences). Data were analyzed with FlowJo software (Ashland, OR). Experiments were conducted at the CNIC-Cellomics Unit. White blood cell populations in mice were analysed using the Abacus junior 30 system (Diatron Group).

**Statistical analysis.** Data are presented as mean±SEM. In experiments comparing two groups, statistical significance was evaluated using unpaired Student's t-test. For multigroup comparisons, a two-way ANOVA with Bonferroni's post-hoc test was performed. The GraphPad Prism 5 software was used for all statistical analyses. P values below 0.05 were deemed significant.

## Results

### **Diet-induced hypercholesterolemia causes a rapid loss of p27 phosphorylation at Ser10 in ECs and aorta that precedes atheroma formation**

It is well established that dyslipidemia causes endothelial dysfunction/activation, triggering the very first steps of atherogenesis [2, 5-7]. To examine whether hypercholesterolemia influences the phosphorylation status of p27 at Ser10, we challenged apoE<sup>-/-</sup> mice with a high-fat diet (HFD) for a very short period (9 days). Under these conditions, fat-fed apoE<sup>-/-</sup> mice developed hypercholesterolemia (Figure 1A) but, similar to control mice fed standard chow, they did not present grossly visible atheromata (data not shown). Consistent with the absence of atherosclerotic plaques, qPCR analysis did not reveal changes in the expression of the leukocyte-specific L-selectin in aorta of control and fat-fed apoE<sup>-/-</sup> mice (Figure 1B). Likewise, expression of adhesion molecules associated with endothelial activation was unchanged when comparing aorta from control and fat-fed mice, with the only exception of VCAM-1 (p=0.0353, Figure 1B). Notably, short term exposure of apoE<sup>-/-</sup> mice to HFD caused a marked loss of p27 phosphorylation at Ser10 in the aortic arch, as revealed by western blotting using anti-p27-phospho-Ser10 (Figure 1C). In agreement with this result, primary mAECs treated with serum from mice fed HFD for 4 days showed a significant reduction of p27 phosphorylation compared with cells treated with control serum (Figure 1D). Of note, both free and total cholesterol levels in serum of mice fed HFD for 4 and 9 days were undistinguishable from those observed after longer exposure to HFD (Supplementary Figure S1). These results demonstrate that, preceding the appearance of macroscopically detectable lesions, high levels of cholesterol in blood are associated with a rapid decrease in p27-phospho-Ser10 in mAECs and aorta of apoE<sup>-/-</sup> mice.

### **Lack of p27 phosphorylation at Ser10 enhances expression of endothelial adhesion molecules**

To further investigate the role of p27-phospho-Ser10 during early atherogenesis, we generated apoE<sup>-/-</sup>p27Ser10Ala mice homozygous for a knock-in alanine substitution at Ser10 that blocks phosphorylation in this residue [30]. These mice exhibit increased atherosclerosis at advanced stages of disease progression [32]. Western blot analysis confirmed the lack of p27-phospho-Ser10 in the aorta of apoE<sup>-/-</sup>p27Ser10Ala mice (Figure 2A). The results of qPCR analysis showed elevated L-selectin, P-selectin, ICAM-1, and VCAM-1 expression in aortas of apoE<sup>-/-</sup>p27Ser10Ala mice fed control diet compared with apoE<sup>-/-</sup> littermates, which reached statistical significance for L-selectin, ICAM-1 and VCAM-1 (Figure 2B). These results suggest that endothelial dysfunction develops in apoE<sup>-/-</sup>p27Ser10Ala mice even in the absence of a proatherogenic dietary challenge.

We next cultured mAECs from p27Ser10Ala and wild-type mice to assess whether impaired p27-phospho-Ser10 was causally linked to early endothelial dysfunction. Western blot analysis confirmed the absence of p27-phospho-Ser10 in mAECs from p27Ser10Ala mice (Figure 2C, left). Results from qPCR analysis showed no differences in P-selectin or ICAM-1 mRNA expression between cells from both genotypes, however, VCAM-1 mRNA expression was significantly increased in p27Ser10Ala mAECs compared with controls (Figure 2C, right). This change in VCAM-1 expression was not accompanied by significant alterations in the protein level of adhesion molecules in different subsets of circulating leukocytes (Figure 2D, top). Likewise, lack of p27-phospho-Ser10 did not alter the number of circulating leukocytes in apoE<sup>-/-</sup> (Figure 2D, bottom) and wild-type (Supplementary Figure S2) backgrounds.

### **Lack of p27 phosphorylation at Ser10 in endothelial cells increases VCAM-1 protein expression and RhoA/ROCK signaling**

We next explored what mechanisms might produce increased VCAM-1 expression in mAECs with defective p27-phospho-Ser10. Given that loss of this phosphorylation activates RhoA/ROCK-dependent signaling in aorta [32], and that this pathway promotes the activation of integrins [40], we examined whether RhoA/ROCK could modulate VCAM-1 overexpression in p27Ser10Ala mAECs. We evaluated by western blotting the phosphorylation status of the ezrin/radixin/moesin proteins (ERM), a reliable marker of RhoA/ROCK signaling [41]. We found an increased phospho-ERM-to-ERM ratio in p27Ser10Ala mutant mAECs relative to wild-type cells (Figure 3A). In accord with mRNA expression studies, we also found increased VCAM-1 protein in p27Ser10Ala mAECs (Figure 3B) without changes in ICAM-1 and P-selectin (Figure 3C). Since RhoA/ROCK induces VCAM-1 expression [40], these findings suggest that defective p27-phospho-Ser10 enhances the expression of VCAM-1 *via* RhoA/ROCK-dependent signaling in mAECs.

### **Lack of p27 phosphorylation at Ser10 stimulates leukocyte-endothelium interaction in arterioles and atherosusceptible arteries *via* RhoA/ROCK activation**

The above findings suggested that leukocyte-EC interactions might be enhanced upon loss of p27-phospho-Ser10. Consistent with this notion, expression of the leukocyte marker, L-selectin, was increased in the aorta of apoE<sup>-/-</sup>p27Ser10Ala mutant mice (Figure 2B). To assess the impact of defective p27-phospho-Ser10 on leukocyte-EC interactions *in vivo*, we next performed intravital microscopy in the cremaster muscle. These studies demonstrated a significant increase in the number of adhered leukocytes in cremasteric arterioles of p27Ser10Ala mice compared with wild-type littermates (Figure 4A).

We next assessed whether higher VCAM-1 expression induced by p27Ser10Ala expression is required for increased leukocyte-EC interactions. To this end, we performed intravital microscopy experiments in mice treated with either control IgG or anti-VCAM-1 antibodies. These experiments revealed that anti-VCAM-1 antibody but not control IgG blunts the excess of leukocyte-EC interactions in p27Ser10Ala mice (Figure 4B). Because p27Ser10Ala mAECs displayed greater VCAM-1 expression, and RhoA/ROCK-dependent signaling induces VCAM-1 expression and promotes leukocyte-EC interactions [42-45], we also investigated the impact of RhoA inhibition. Treatment of p27Ser10Ala mice with the selective RhoA/ROCK inhibitor fasudil significantly reduced leukocyte adhesion to the levels seen in wild-type controls (Figure 4A).

Luminal recruitment appears to be the major route of leukocyte infiltration in the subendothelial space, which precedes early atheroma build-up [3-9]. Using high-speed intravital fluorescent microscopy and rhodamine 6G labeling *in vivo* [3], we quantified leukocyte rolling within carotid arteries of apoE<sup>-/-</sup>p27Ser10Ala and apoE<sup>-/-</sup> mice fed either control diet or HFD for 2 weeks. As expected, high-fat feeding significantly increased leukocyte rolling activity in apoE<sup>-/-</sup> mice expressing either wild-type or mutant p27, but we noted greater rolling in p27Ser10Ala mice fed either type of diet compared with their wild-type counterparts (Figure 5A).

After rolling, leukocytes adhere firmly to the endothelium and rapidly change their morphology and redistribute specific receptors [3-9]. At later stages, leukocytes crawl on the endothelium in search of areas permissive for extravasation, and are finally recruited into the intima of the artery [3-9]. To assess whether increased leukocyte rolling upon loss of p27-phospho-Ser10 was accompanied by augmented leukocyte recruitment into atherogenic arteries, we performed adoptive transfer experiments using bone marrow-derived leukocytes from Mafia-apoE<sup>-/-</sup> mice, which express GFP in myeloid cells [3, 33]. Thus, cells were transferred into apoE<sup>-/-</sup>p27Ser10Ala and apoE<sup>-/-</sup> mice, and GFP expression in the aorta was determined as a metric of homing of Mafia-apoE<sup>-/-</sup> leukocytes. qPCR analysis demonstrated significantly greater GFP expression in aorta from apoE<sup>-/-</sup>p27Ser10Ala relative to apoE<sup>-/-</sup> mice, and this difference was abolished upon treatment with fasudil (Figure 5B).

### **Lack of p27 phosphorylation at Ser10 accelerates early atherosclerosis development *via* RhoA/ROCK activation**

The *in vivo* studies presented thus far were performed in mice fed standard chow or challenged with HFD for very short periods of time; consequently, mice did not exhibit significant plaque build-up. To investigate whether increased leukocyte recruitment upon loss of p27-phospho-Ser10 accelerates early atherosclerotic lesion development, Mafia-apoE<sup>-/-</sup> and Mafia-apoE<sup>-/-</sup>p27Ser10Ala mice were challenged with HFD for 4 weeks, and aortic sinus cross-sections were analyzed. Under these conditions, both groups of mice presented early lesions consisting of fatty streaks containing predominantly F4/80-immunoreactive macrophages ([Supplementary Figure S4](#)). Importantly, atherosclerosis burden was significantly augmented in Mafia-apoE<sup>-/-</sup>p27Ser10Ala mice compared with controls (Figure 6A, top). Moreover, aortic VCAM-1 expression and the accumulation of GFP+ leukocytes were increased in fat-fed Mafia-apoE<sup>-/-</sup>p27Ser10Ala mice (Figure 5B, top). In agreement with our earlier findings, fasudil treatment blunted the increase of atherosclerosis (Figure 6A, bottom) and aortic VCAM-1 expression and GFP+ leukocyte accumulation (Figure 6B, bottom) associated with loss of p27-phospho-Ser10.

## Discussion

Previous studies have demonstrated a protective role of p27 in the development of advanced atherosclerotic plaques in apoE<sup>-/-</sup> mice through proliferation-dependent and proliferation-independent mechanisms [12, 13, 16, 32]. However, whether p27 regulates atherosclerosis development at initial stages when neointimal cell proliferation is not yet prominent, was unknown. Therefore, examining p27 proliferation-independent functions, including those regulated through posttranslational modifications, are of interest in this particular context. In the present study, we investigated the role of p27-phospho-Ser10 in early atherosclerosis by challenging apoE<sup>-/-</sup> mice with HFD for different periods of time: very short exposure (4, 9 days), which was sufficient to cause maximum hypercholesterolemia but failed to induce the appearance of macroscopically visible lesions; short exposure (14 days) to quantify leukocyte-EC interactions *in vivo* in very incipient plaques; and long exposure (28 days) to quantify atherosclerosis burden at early stages of disease progression. We initially observed that hypercholesterolemia induced by short-term exposure (9 days) to HFD was associated with a reduction in p27-phospho-Ser10 in the aorta of apoE<sup>-/-</sup> mice. This loss occurred very rapidly, preceding both the upregulation of adhesion molecules that trigger leukocyte recruitment and also the development of macroscopically visible lesions. Downregulation of p27 phosphorylation was also observed in mAECs challenged with serum from apoE<sup>-/-</sup> mice fed HFD for 4 days, suggesting that hypercholesterolemia may be a factor contributing to p27 dephosphorylation. Importantly, our findings in mAECs and aorta expressing the non-phosphorylated form of p27 establish a causal relationship between defective p27-phospho-Ser10 and EC activation since expression of VCAM-1, a key positive regulator of leukocyte-endothelium interactions in atherosclerotic arteries [3-9], is increased in p27Ser10Ala aorta and mAECs.

The finding that defective p27-phospho-Ser10 leads to increased expression of VCAM-1 and of the leukocyte marker L-selectin (CD62L) in the aorta of apoE<sup>-/-</sup>p27Ser10Ala mutant mice, prompted us to examine whether loss of this post-translational modification increases leukocyte infiltration. *In vitro* adhesion assays, *in vivo* intravital microscopy in carotid artery and cremaster muscle arterioles, and *in vivo* homing studies in aorta revealed augmented leukocyte-EC interactions and leukocyte recruitment upon expression of p27Ser10Ala. It is noteworthy that the increase in leukocyte rolling in the carotid artery induced by defective p27-phospho-Ser10 expression was diminished in apoE<sup>-/-</sup>p27Ser10Ala and apoE<sup>-/-</sup> mice challenged with HFD, when compared with identical groups fed standard chow. This is presumably due to the loss of p27-phospho Ser10 that occurs rapidly in fat-fed apoE<sup>-/-</sup> mice. The pathological relevance of increased aortic VCAM-1 expression and leukocyte-EC interaction upon loss of p27-phospho-Ser10 is underscored by the observation that apoE<sup>-/-</sup>p27Ser10Ala mice fed HFD for 4 weeks exhibited larger macrophage-rich fatty streaks. This increase in macrophage accumulation correlated with enhanced aortic VCAM-1 expression, and augmented GFP+ myeloid leukocyte homing into the aortic arch of apoE<sup>-/-</sup>p27Ser10Ala-Mafia mice. The use of the Mafia GFP-reporter mouse in adoptive transfer studies allowed us to demonstrate a causal relationship between p27Ser10Ala expression and increased recruitment of leukocytes into early fatty streaks since transfer of GFP+ myeloid cells was significantly increased in aorta of recipient apoE<sup>-/-</sup>p27Ser10Ala mice.

During vascular inflammation, the VCAM-1 integrin is one of a plethora of induced adhesion molecules (e.g. selectins, chemokines, integrins) that differentially mediate interactions during the distinct phases of recruitment [8]. We have shown here that treatment with anti-VCAM-1 antibody blunts the excess of leukocyte-EC interactions in cremasteric arterioles of p27Ser10Ala mice. Activation of the RhoA/ROCK pathway has been linked to vascular inflammation, leukocyte recruitment, and expression of adhesion molecules in ECs, particularly those involved in the slow rolling and arrest phases [40, 42-44, 46-49]. Disruption of RhoA/ROCK signaling, using pharmacological inhibitors or through genetic ablation of individual components of the pathway, significantly reduces neointimal thickening in rat and mouse

models of atherosclerosis, balloon angioplasty and artery ligation [45, 50-53]. We demonstrate here that the absence of p27-phospho-Ser10 leads to an increase in the phospho-ERM/ERM ratio in mAECs. The increase in this *bona fide* marker of RhoA/ROCK signaling coincided with higher levels of VCAM-1 expression and enhanced adhesion of leukocytes to p27Ser10Ala mAECs *in vitro* and in cremaster muscle arterioles *in vivo*. These differences were abolished after treatment with the RhoA/Rock inhibitor fasudil. Similarly, fasudil abolished the increase of aortic VCAM-1 expression, leukocyte homing and atherosclerosis burden in apoE<sup>-/-</sup> p27Ser10Ala mice.

Regarding the mechanism through which lack of p27-phospho-Ser10 leads to increased RhoA/ROCK-dependent signaling, it has been shown that p27 interacts directly with RhoA and inhibits its function [18, 54]. Moreover, lack of p27-phospho-Ser10 in several cell types restrains p27's exit from the nucleus to the cytoplasm leading to reduced level of this tumor suppressor in the cytoplasm [24, 25, 27, 31, 32, 55], where the interaction p27-RhoA occurs. This could explain, at least in part, the enhancement of RhoA/ROCK activity in cells expressing p27Ser10Ala. Consistent with this possibility, we found less accumulation of p27 in the cytoplasm of mAECs lacking p27-phospho-Ser10 (Supplementary Figure S3). Taken together, these results suggest that reduced level of cytoplasmic p27 in p27Ser10Ala mAECs may enhance RhoA/ROCK activity and the ensuing VCAM-1 induction by diminishing the interaction between p27 and RhoA. However, further studies are required to ascertain the exact mechanism by which p27 phosphorylation at Ser10 modulates the RhoA/ROCK pathway.

In summary, our findings establish for the first time a causal link between defective p27 phosphorylation and RhoA/ROCK activation that promotes EC dysregulation, leukocyte recruitment and the development of early atherosclerotic lesions. These observations extend the results of previous studies by others demonstrating that p27 regulates the RhoA/ROCK pathway [18]. They also build on our recent studies showing that loss of p27-phospho-Ser10 exacerbates advanced atherosclerosis in apoE<sup>-/-</sup> p27Ser10Ala mice coinciding with augmented foam cell formation owing to increased RhoA/ROCK activity in macrophages [32]. It is also important to note that our present findings, taken together with previous studies in apoE<sup>-/-</sup> mice lacking p27 [12, 13, 16] or p27-phospho-Ser10 [32], demonstrate that p27 affects all stages of plaque formation: from the early fatty streaks to complex plaques, through cell cycle-dependent and cell cycle-independent mechanisms that operate in different cell types (vascular smooth muscle cells, macrophages and ECs). These properties could therefore be exploited to develop versatile therapeutics targeting p27 to inhibit atherogenesis at all stages of lesion development.

## Conclusions

p27 undergoes rapid dephosphorylation at Ser10 in aorta of fat-fed apoE<sup>-/-</sup> preceding development of macroscopically-visible lesions. Defective p27-phospho-Ser10 enhances the expression of adhesion molecules in aorta of apoE<sup>-/-</sup> mice and endothelial cells, and augments endothelial-leukocyte interactions, leukocyte recruitment and the development of early atherosclerosis development. Treatment with the RhoA/ROCK inhibitor fasudil blunts the pro-atherogenic effects of defective p27-phospho-Ser10.

## **Acknowledgements**

We thank V. Zorita, I. Ortega, J. Mateos, the Cellomic and Comparative Medicine Units at CNIC for animal care, A. Hidalgo for help in experimental design and for providing access to the intravital microscopy platform, and Kenneth McCreath for English editing. Work supported by grants from the Spanish Ministry of Economy and Competitiveness (MINECO) (SAF2010-16044, SAF2013-46663-R), Fondo Europeo de Desarrollo Regional (FEDER), and Instituto de Salud Carlos III (RD12/0042/0028). P.M-S. is supported by a FPU predoctoral fellowship from MINECO. The Centro Nacional de Investigaciones Cardiovasculares (CNIC) is supported by the MINECO and the Pro-CNIC Foundation.

## **Conflict of interest**

None.



## References

1. Roger VL, Go AS, Lloyd-Jones DM, Benjamin EJ, Berry JD, Borden WB, et al. Executive summary: heart disease and stroke statistics--2012 update: a report from the American Heart Association. *Circulation*. 2012;125(1):188-97.
2. Libby P, Ridker PM, Hansson GK. Progress and challenges in translating the biology of atherosclerosis. *Nature*. 2011;473(7347):317-25.
3. Chevre R, Gonzalez-Granado JM, Megens RT, Sreeramkumar V, Silvestre-Roig C, Molina-Sanchez P, et al. High-Resolution Imaging of Intravascular Atherogenic Inflammation in Live Mice. *Circ Res*. 2014;114(5):770-9.
4. Binder CJ, Chang MK, Shaw PX, Miller YI, Hartvigsen K, Dewan A, et al. Innate and acquired immunity in atherogenesis. *Nat Med*. 2002;8(11):1218-26.
5. Hansson GK. Inflammation, atherosclerosis, and coronary artery disease. *New Engl J Med*. 2005;352(16):1685-95.
6. Lusis AJ. Atherosclerosis. *Nature*. 2000;407(6801):233-41.
7. Glass CK, Witztum JL. Atherosclerosis: The Road Ahead. *Cell*. 2001;104:503-16.
8. Galkina E, Ley K. Leukocyte influx in atherosclerosis. *Curr Drug Targets*. 2007;8(12):1239-48.
9. Swirski FK, Nahrendorf M. Leukocyte behavior in atherosclerosis, myocardial infarction, and heart failure. *Science*. 2013;339(6116):161-6.
10. Eriksson EE. Intravital microscopy on atherosclerosis in apolipoprotein e-deficient mice establishes microvessels as major entry pathways for leukocytes to advanced lesions. *Circulation*. 2011;124(19):2129-38.
11. Fuster JJ, Fernandez P, Gonzalez-Navarro H, Silvestre C, Abu Nabah YN, Andres V. Control of cell proliferation in atherosclerosis: insights from animal models and human studies. *Cardiovasc Res*. 2010;86:254-64
12. Diez-Juan A, Andres V. The growth suppressor p27Kip1 protects against diet-induced atherosclerosis. *FASEB J*. 2001;15(11):1989-95.
13. Diez-Juan A, Perez P, Aracil M, Sancho D, Bernad A, Sanchez-Madrid F, et al. Selective inactivation of p27Kip1 in hematopoietic progenitor cells increases neointimal macrophage proliferation and accelerates atherosclerosis. *Blood*. 2004;103(1):158-61.
14. Chen D, Krasinski K, Sylvester A, Chen J, Nisen PD, Andrés V. Downregulation of cyclin-dependent kinase 2 activity and cyclin A promoter activity in vascular smooth muscle cells by p27(KIP1), an inhibitor of neointima formation in the rat carotid artery. *J Clin Invest*. 1997;99:2334-41.
15. Tanner FC, Boehm M, Akyurek LM, San H, Yang Z-Y, Tashiro J, et al. Differential Effects of the Cyclin-Dependent Kinase Inhibitors p27Kip1, p21Cip1, and p16Ink4 on Vascular Smooth Muscle Cell Proliferation. *Circulation*. 2000;101(17):2022-5.
16. Akyürek LM, Boehm M, Olive M, Zhou A-X, San H, Nabel EG. Deficiency of cyclin-dependent kinase inhibitors p21Cip1 and p27Kip1 accelerates atherogenesis in apolipoprotein E-deficient mice. *Biochem Bioph Res Co* 2010;396(2):359-63.
17. Santulli G, Wronska A, Uryu K, Diacovo TG, Gao M, Marx SO, et al. A selective microRNA-based strategy inhibits restenosis while preserving endothelial function. *J Clin Invest*. 2014;124(9):4102-14.
18. Besson A, Gurian-West M, Schmidt A, Hall A, Roberts JM. p27Kip1 modulates cell migration through the regulation of RhoA activation. *Genes Dev*. 2004;18(8):862-76.
19. Diez-Juan A, Andres V. Coordinate control of proliferation and migration by the p27Kip1/Cyclin-Dependent Kinase/Retinoblastoma pathway in vascular smooth muscle cells and fibroblasts. *Circ Res*. 2003;92(4):402-10.

20. McAllister SS, Becker-Hapak M, Pintucci G, Pagano M, Dowdy SF. Novel p27kip1 C-terminal scatter domain mediates Rac-dependent cell migration independent of cell cycle arrest functions. *Mol Cell Biol.* 2003;23(1):216-28.
21. Pippa R, Espinosa L, Gudem G, Garcia-Escudero R, Dominguez A, Orlando S, et al. p27Kip1 represses transcription by direct interaction with p130/E2F4 at the promoters of target genes. *Oncogene.* 2012;31(38):4207-20.
22. Castro C, Diez-Juan A, Cortes MJ, Andres V. Distinct regulation of mitogen-activated protein kinases and p27Kip1 in smooth muscle cells from different vascular beds. A potential role in establishing regional phenotypic variance. *J Biol Chem.* 2003;278(7):4482-90.
23. Besson A, Dowdy SF, Roberts JM. CDK Inhibitors: Cell Cycle Regulators and Beyond. *Dev Cell.* 2008;14(2):159-69.
24. Besson A, Gurian-West M, Chen X, Kelly-Spratt KS, Kemp CJ, Roberts JM. A pathway in quiescent cells that controls p27Kip1 stability, subcellular localization, and tumor suppression. *Genes Dev.* 2006;20(1):47-64.
25. Boehm M, Yoshimoto T, Crook MF, Nallamshetty S, True A, Nabel GJ, et al. A growth factor-dependent nuclear kinase phosphorylates p27Kip1 and regulates cell cycle progression. *EMBO J.* 2002;21(13):3390-401.
26. Deng X, Mercer SE, Shah S, Ewton DZ, Friedman E. The Cyclin-dependent Kinase Inhibitor p27Kip1 Is Stabilized in G0 by Mirk/dyrk1B Kinase. *J Biol Chem.* 2004;279(21):22498-504.
27. Ishida N, Hara T, Kamura T, Yoshida M, Nakayama K, Nakayama KI. Phosphorylation of p27 Kip1 on Serine 10 Is Required for Its Binding to CRM1 and Nuclear Export. *Journal of Biological Chemistry.* 2002;277(17):14355-8.
28. Ishida N, Kitagawa M, Hatakeyama S, Nakayama K-i. Phosphorylation at serine 10, a major phosphorylation site of p27Kip1, increases its protein stability. *J Biol Chem.* 2000;275(33):25146-54.
29. Kawauchi T, Chihama K, Nabeshima Y-i, Hoshino M. Cdk5 phosphorylates and stabilizes p27kip1 contributing to actin organization and cortical neuronal migration. *Nat Cell Biol.* 2006;8(1):17-26.
30. Kotake Y, Nakayama K, Ishida N, Nakayama KI. Role of serine 10 phosphorylation in p27 stabilization revealed by analysis of p27 knock-in mice harboring a serine 10 mutation. *J Biol Chem.* 2005;280(2):1095-102.
31. Rodier G, Montagnoli A, Di Marcotullio L, Coulombe P, Draetta GF, Pagano M, et al. p27 cytoplasmic localization is regulated by phosphorylation on Ser10 and is not a prerequisite for its proteolysis. *EMBO J.* 2001;20(23):6672-82.
32. Fuster JJ, Gonzalez-Navarro H, Vinue A, Molina-Sanchez P, Andres-Manzano MJ, Nakayama KI, et al. Deficient p27 phosphorylation at serine 10 increases macrophage foam cell formation and aggravates atherosclerosis through a proliferation-independent mechanism. *Arterioscler Thromb Vasc Biol.* 2011;31(11):2455-63.
33. Burnett SH, Kershen EJ, Zhang J, Zeng L, Straley SC, Kaplan AM, et al. Conditional macrophage ablation in transgenic mice expressing a Fas-based suicide gene. *J Leukoc Biol.* 2004;75(4):612-23.
34. Golde WT, Gollobin P, Rodriguez LL. A rapid, simple, and humane method for submandibular bleeding of mice using a lancet. *Lab Anim (NY).* 2005;34(9):39-43.
35. Mahabeleshwar GH, Somanath PR, Byzova TV. Methods for isolation of endothelial and smooth muscle cells and in vitro proliferation assays. *Methods Mol Med.* 2006;129:197-208.
36. Soleimani M, Nadri S. A protocol for isolation and culture of mesenchymal stem cells from mouse bone marrow. *Nat Protoc.* 2009;4(1):102-6.

37. Doring Y, Drechsler M, Wantha S, Kemmerich K, Lievens D, Vijayan S, et al. Lack of neutrophil-derived CRAMP reduces atherosclerosis in mice. *Circ Res*. 2012;110(8):1052-6.
38. Sanz-González SM, Melero-Fernández-de-Mera R, Malek NP, Andrés V. Atheroma development in apolipoprotein E-null mice is not regulated by phosphorylation of p27Kip1 on threonine 187. *J Cell Biochem*. 2006;97(4):735-43.
39. Gonzalez-Navarro H, Vinue A, Vila-Caballer M, Fortuno A, Beloqui O, Zalba G, et al. Molecular Mechanisms of Atherosclerosis in Metabolic Syndrome: Role of Reduced IRS2-Dependent Signaling. *Arterioscler Thromb Vasc Biol*. 2008;28(12):2187-94.
40. Kawanami D, Matoba K, Okada R, Tsukamoto M, Kinoshita J, Ishizawa S, et al. Fasudil inhibits ER stress-induced VCAM-1 expression by modulating unfolded protein response in endothelial cells. *Biochem Biophys Res Commun*. 2013;435(2):171-5.
41. Rekhter M, Chandrasekhar K, Gifford-Moore D, Huang X, Rutherford P, Hanson J, et al. Immunohistochemical analysis of target proteins of Rho-kinase in a mouse model of accelerated atherosclerosis. *Exp Clin Card*. 2007;12(4):169-74.
42. Slotta JE, Braun OO, Menger MD, Thorlacius H. Fasudil, a Rho-kinase inhibitor, inhibits leukocyte adhesion in inflamed large blood vessels in vivo. *Inflamm Res*. 2006;55(9):364-7.
43. Thorlacius K, Slotta JE, Laschke MW, Wang Y, Menger MD, Jeppsson B, et al. Protective effect of fasudil, a Rho-kinase inhibitor, on chemokine expression, leukocyte recruitment, and hepatocellular apoptosis in septic liver injury. *J Leukoc Biol*. 2006;79(5):923-31.
44. Wang QM, Stalker TJ, Gong Y, Rikitake Y, Scalia R, Liao JK. Inhibition of Rho-kinase attenuates endothelial-leukocyte interaction during ischemia-reperfusion injury. *Vasc Med*. 2012;17(6):379-85.
45. Wu DJ, Xu JZ, Wu YJ, Jean-Charles L, Xiao B, Gao PJ, et al. Effects of fasudil on early atherosclerotic plaque formation and established lesion progression in apolipoprotein E-knockout mice. *Atherosclerosis*. 2009;207(1):68-73.
46. Loirand G, Guerin P, Pacaud P. Rho Kinases in Cardiovascular Physiology and Pathophysiology. *Circ Res*. 2006;98(3):322-34.
47. Rolfe BE, Worth NF, World CJ, Campbell JH, Campbell GR. Rho and vascular disease. *Atherosclerosis*. 2005;183(1):1-16.
48. Zhou Q, Liao JK. Rho Kinase: an important mediator of atherosclerosis and vascular disease. *Curr Pharm Des*. 2009;15(27):3108-15.
49. Wang H-W, Liu P-Y, Oyama N, Rikitake Y, Kitamoto S, Gitlin J, et al. Deficiency of ROCK1 in bone marrow-derived cells protects against atherosclerosis in LDLR<sup>-/-</sup> mice. *FASEB J*. 2008;22(10):3561-70.
50. Ma Z, Zhang J, Du R, Ji E, Chu L. Rho kinase inhibition by fasudil has anti-inflammatory effects in hypercholesterolemic rats. *Biol Pharm Bull*. 2011;34(11):1684-9.
51. Noma K, Rikitake Y, Oyama N, Yan G, Alcaide P, Liu P-Y, et al. ROCK1 mediates leukocyte recruitment and neointima formation following vascular injury. *J Clin Invest*. 2008;118(5):1632-44.
52. Sawada N, Itoh H, Ueyama K, Yamashita J, Doi K, Chun T-H, et al. Inhibition of Rho-Associated Kinase Results in Suppression of Neointimal Formation of Balloon-Injured Arteries. *Circulation*. 2000;101(17):2030-3.
53. Mallat Z, Gojova A, Sauzeau V, Brun V, Silvestre J-S, Esposito B, et al. Rho-associated protein kinase contributes to early atherosclerotic lesion formation in mice. *Circ Res*. 2003;93(9):884-8.

54. Larrea MD, Hong F, Wander SA, da Silva TG, Helfman D, Lannigan D, et al. RSK1 drives p27Kip1 phosphorylation at T198 to promote RhoA inhibition and increase cell motility. *Proc Natl Acad Sci U S A.* 2009;106(23):9268-73.
55. Gui P, Labrousse A, Van Goethem E, Besson A, Maridonneau-Parini I, Le Cabec V. Rho/ROCK pathway inhibition by the CDK inhibitor p27(kip1) participates in the onset of macrophage 3D-mesenchymal migration. *J Cell Sci.*127(Pt 18):4009-23.

## Figure legends

**Figure 1: Hypercholesterolemia in apoE<sup>-/-</sup> mice is associated with reduced phosphorylation of p27 at Ser10.** (A, B) apoE<sup>-/-</sup> mice were fed either control diet (CD, n=6) or a high-fat diet (HFD, n=5) for 9 days. (A) Serum cholesterol level. (B) qPCR analysis of adhesion molecules in the aortic arch. (C) Representative western blot of aortic arch (tissue essentially free of atheroma and pooled from 6 mice of each group). The relative p27-phospho-S10/p27 ratio is indicated below (mean ± SEM of 3 blots performed with the same pools). Results are normalized to control diet (=1). p27 ser10-P: p27 phosphorylated in Ser10. (D) Representative western blot of serum-starved mAECs treated for 30 min and 6 h with medium containing 10% of serum from apoE<sup>-/-</sup> mice fed CD or HFD for 4 days. The graph shows the p27 ser10-P/p27 ratio averaged from two independent experiments (each using serum pooled from two mice in each condition).

**Figure 2: Lack of p27 phosphorylation at Ser10 increases adhesion molecule expression in aorta and primary endothelial cells.** (A, B) apoE<sup>-/-</sup> and apoE<sup>-/-</sup> p27Ser10Ala mice were fed standard chow. (A) Aortic arch tissue essentially free of atheroma was obtained from 3 mice of each genotype and analyzed by western blot. A representative blot of one aorta of each genotype is shown. (B) qPCR analysis of adhesion molecule expression in aortic arch (n=2 pools from 2-3 mice). (C) Wild-type and p27Ser10Ala mAEC protein extracts were assessed by western blot (left) or qPCR (right, n=2 pools from 8 mice). (D) TOP: Flow cytometry analysis of adhesion molecule expression: L-Selectin (CD62L), Mac-1 (CD11b), VLA-4 (CD49d) and PSGL-1 in total white blood cells (WBC) and in different leukocyte subsets from Mafia-apoE<sup>-/-</sup> and Mafia-apoE<sup>-/-</sup>p27Ser10Ala mice (n=5-6 mice). MON: monocytes; NEU: neutrophils; LYM: lymphocytes. BOTTOM: Total number of WBC and percentage of monocytes, neutrophils and lymphocytes in blood of apoE<sup>-/-</sup> (n=9) and apoE<sup>-/-</sup>p27Ser10Ala (n=7) mice.

**Figure 3: Lack of p27 phosphorylation at Ser10 increases RhoA/ROCK signaling and VCAM-1 expression in primary endothelial cells.** Protein was extracted from wild-type and p27Ser10Ala mAECs and levels of the indicated proteins were assessed by western blot. Two independent cultures of mAECs were obtained for each genotype. Each culture was prepared from a pool of 6 aortas (pool 1 and pool 2) and was analyzed in 2 western blots which were quantified as follows. Each blot included lanes loaded with samples prepared from each of the two wild-type cell pools and each of the two p27Ser10Ala pools, so that conditions were replicated within the blot. In addition, the blot was repeated with the same samples, giving methodological replicates between the duplicate blots. Mean values were first calculated for the methodological replicates from the corresponding lanes in blot 1 and blot 2 (e.g. wild-type pool 1 from blot 1 and wild-type pool 1 from blot 2). These values were then used to calculate the overall mean value for each condition (=the mean of the mean values for pool 1 and pool 2) with its error bars, as shown in the graph. The bands shown in A and B belong to the same gel but lanes were reorganized for easier comprehension.

**Figure 4: Lack of p27 phosphorylation at Ser10 promotes the adhesion of leukocytes in arterioles through a mechanism mediated by RhoA/ROCK and VCAM-1.** Intravital microscopy of cremaster muscle from p27Ser10Ala or wild-type mice to quantify leukocyte-arteriole wall interactions 4 hours after TNF $\alpha$  injection. (A) The experiment was performed in animals untreated (n=11 wild-type and n=10 p27Ser10Ala arterioles from 4 animals each group) or treated with fasudil (n=21 wild-type and n=21 p27Ser10Ala arterioles from 7 animals each

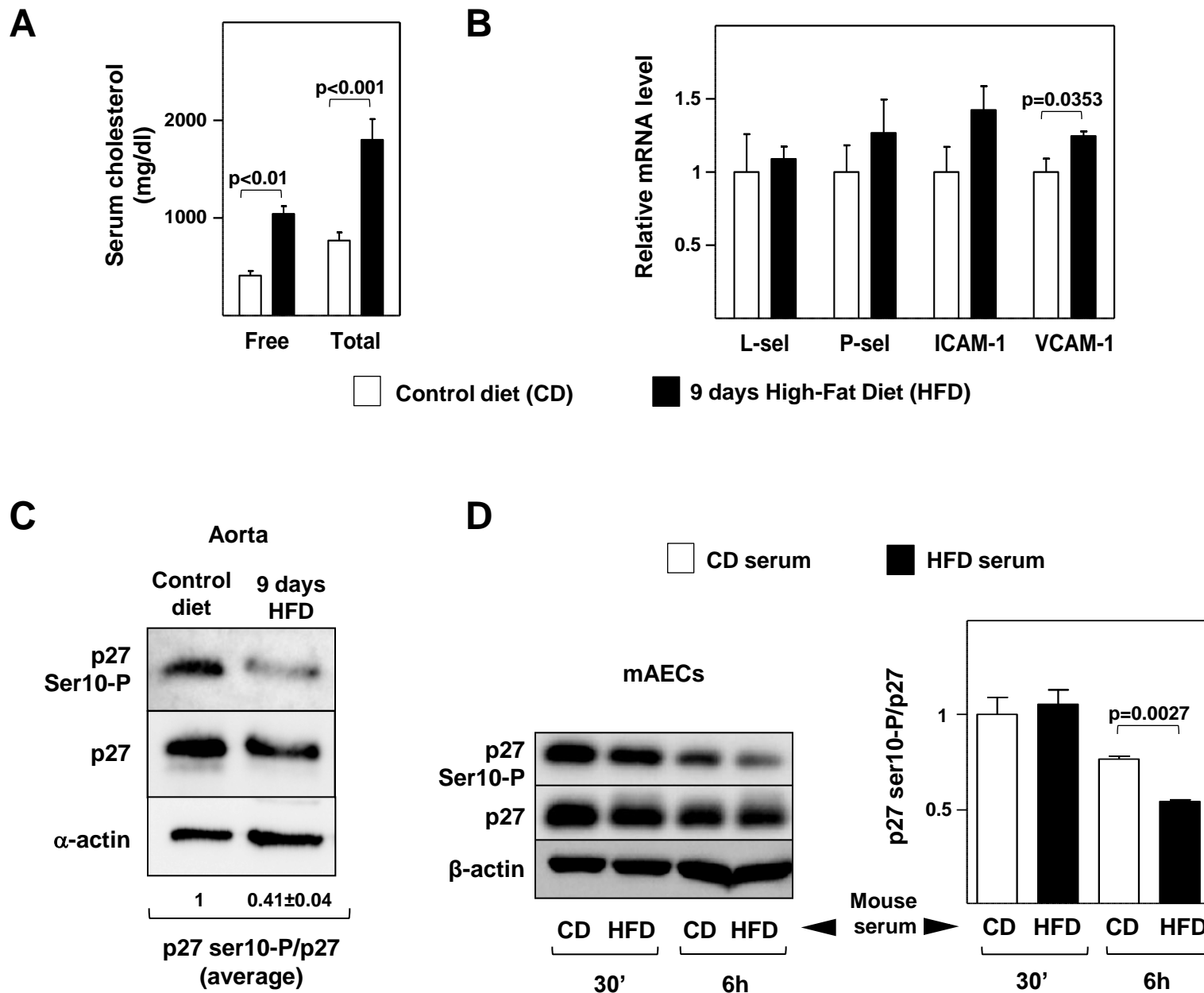
group). Results are represented relative to control wild-type mice (=1). **(B)** The experiment was performed in animals treated with either IgG isotype control (n=12 arterioles from 4 wild-type mice and n=9 arterioles from 3 p27Ser10Ala mice) or  $\alpha$ -VCAM-1 antibody (n=12 arterioles from 4 mice of each genotype). The images show representative fields with leukocytes adhered to endothelium identified with white arrows.

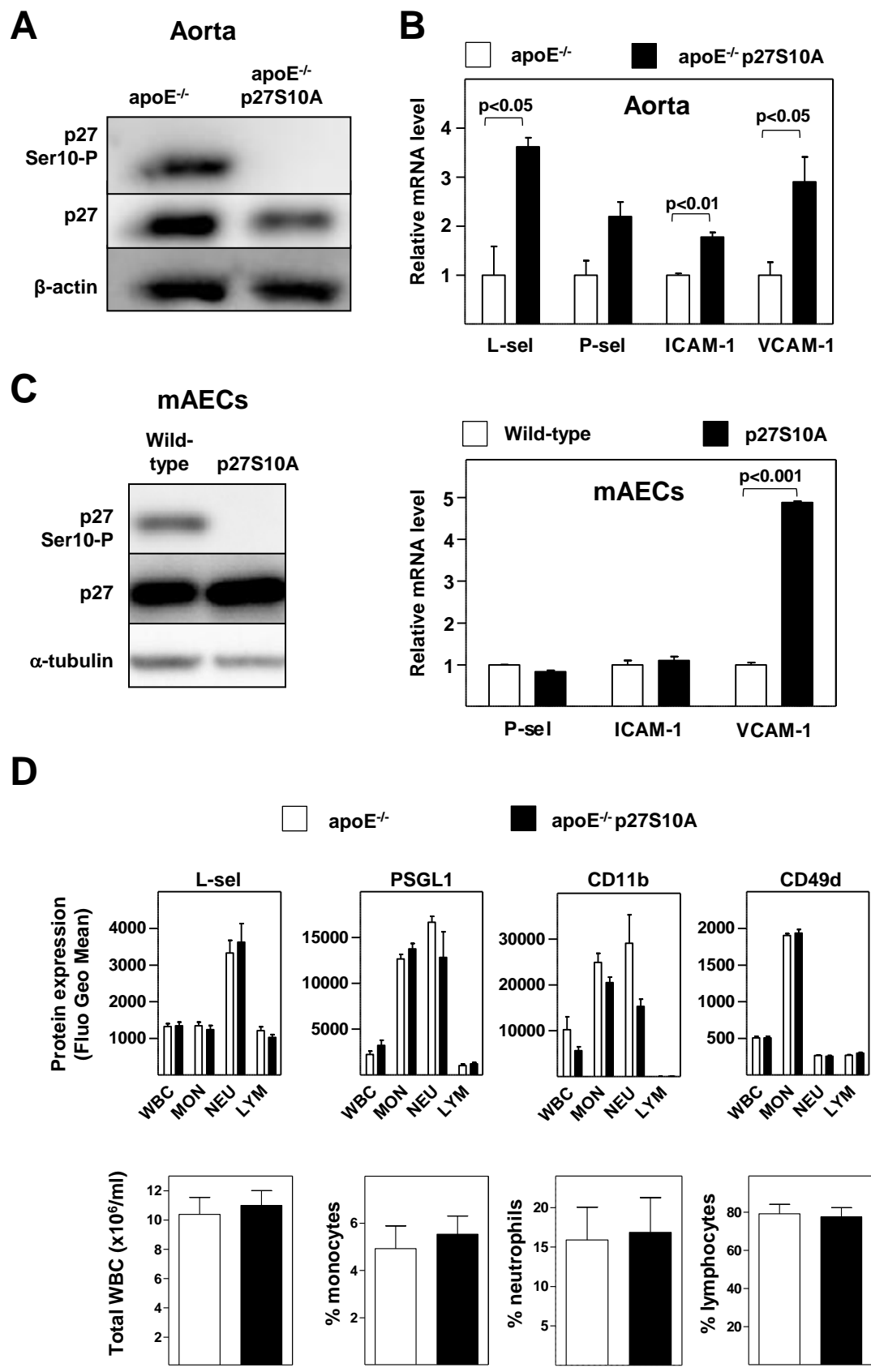
**Figure 5: Lack of p27 phosphorylation at Ser10 promotes the adhesion of leukocytes in atherosusceptible arteries through RhoA/ROCK signaling.** **(A)** High-speed intravital fluorescent microscopy to quantify leukocyte recruitment into carotid artery during early atherogenesis. Three-month-old apoE<sup>-/-</sup> and apoE<sup>-/-</sup>p27Ser10Ala mice were fed HFD for 2 weeks and were injected with rhodamine 6G to label blood cells prior to intravital microscopy. Images show representative fields with leukocytes rolling on the endothelium at the level of the carotid bifurcation. Scale bar: 25  $\mu$ m. The graph shows the number of rolling leukocytes in the carotid bifurcation (n=7-21 fields from 5 mice in each group). **(B)** GFP+ myeloid leukocytes isolated from bone marrow of apoE<sup>-/-</sup>Mafia mice were intravenously injected into apoE<sup>-/-</sup> or apoE<sup>-/-</sup>p27Ser10Ala mice to study their homing into aorta. Two days after adoptive transfer, the level of GFP mRNA in the aortic arch of recipient mice was quantified by qPCR. Experiments were performed in untreated and in fasudil-treated mice (n=4-6 mice).

**Figure 6: Lack of p27 phosphorylation at Ser10 accelerates early atherogenesis through RhoA/ROCK signaling.** Mafia-apoE<sup>-/-</sup> and Mafia-apoE<sup>-/-</sup>p27Ser10Ala mice were fed HFD for 4 weeks to quantify early atherosclerosis. Mafia background was used to quantify the accumulation of GFP+ myeloid cells in aorta. TOP: control mice; BOTTOM: mice treated with fasudil during HFD. **(A)** Representative images of atherosclerotic aortic sinus cross-sections stained with hematoxylin/eosin and quantification of atherosclerosis burden (n=9 control and n=10-11 fasudil-treated mice). **(B)** qPCR analysis of VCAM-1 and GFP expression in aorta (n=4-5 control and fasudil-treated mice).

Figure 1

Figure 1

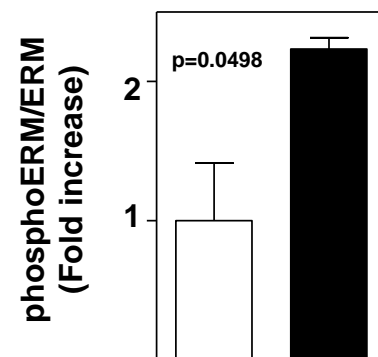
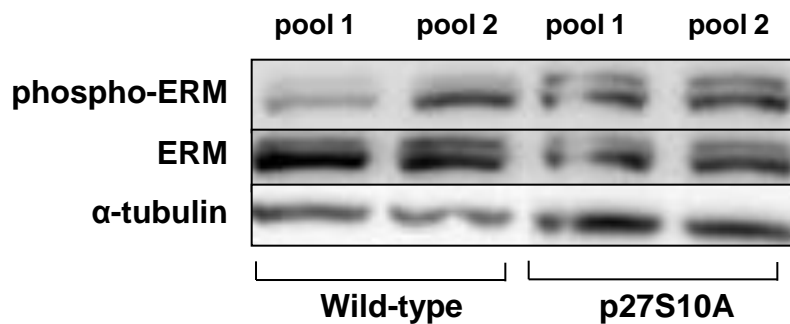




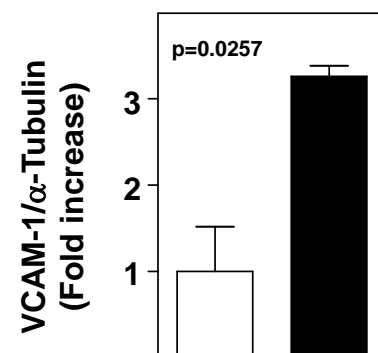
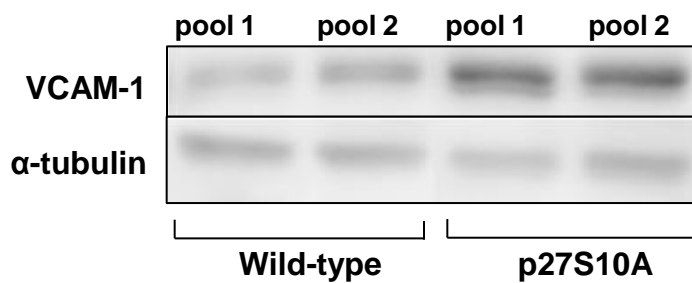


□ Wild-type      ■ p27S10A

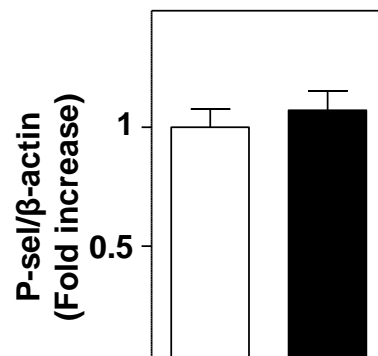
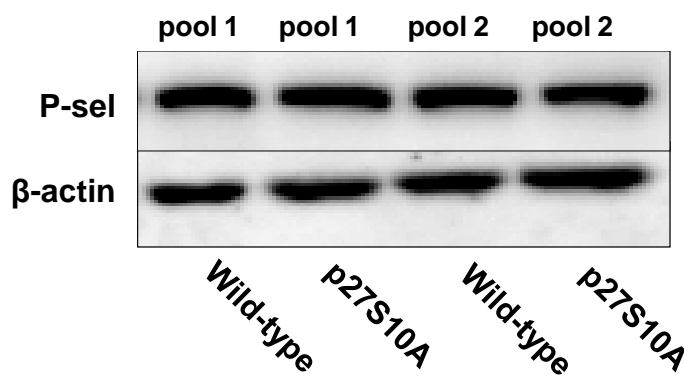
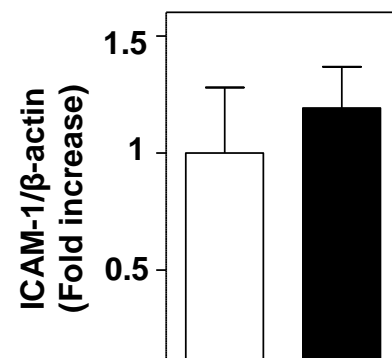
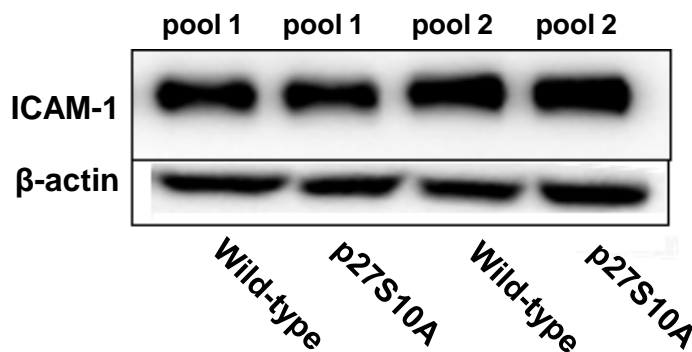
A



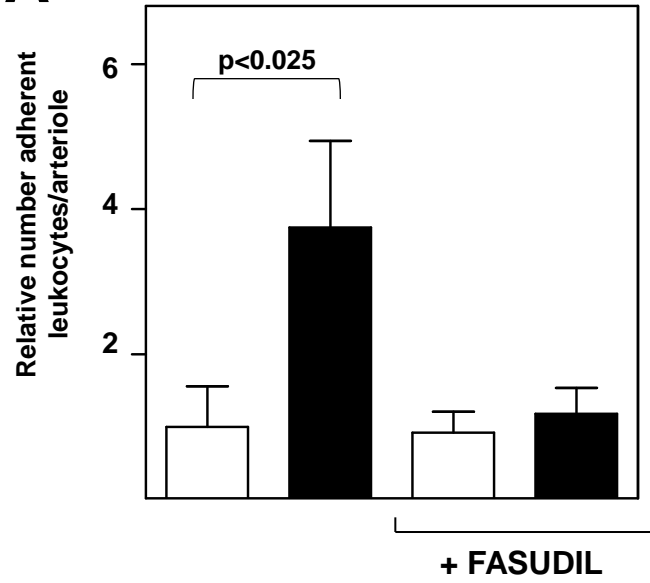
B



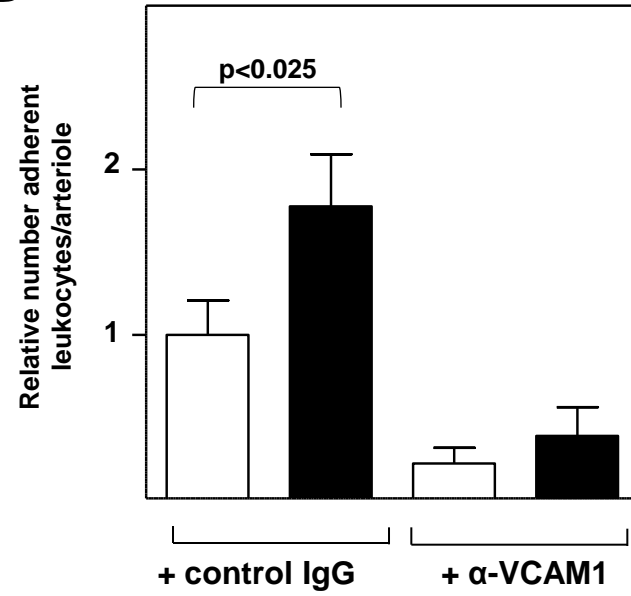
C



**A**

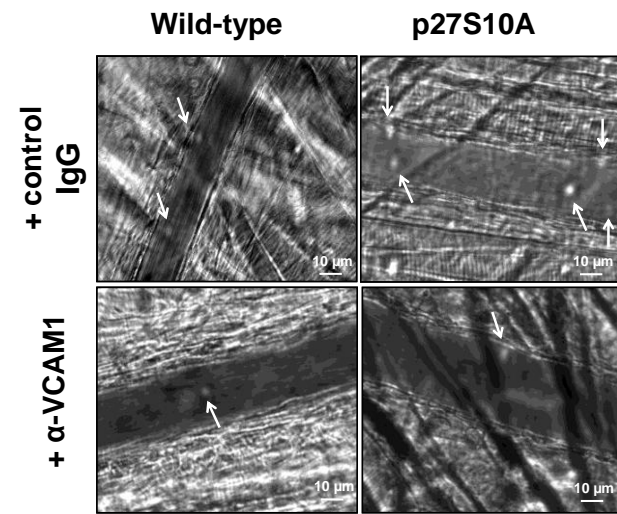
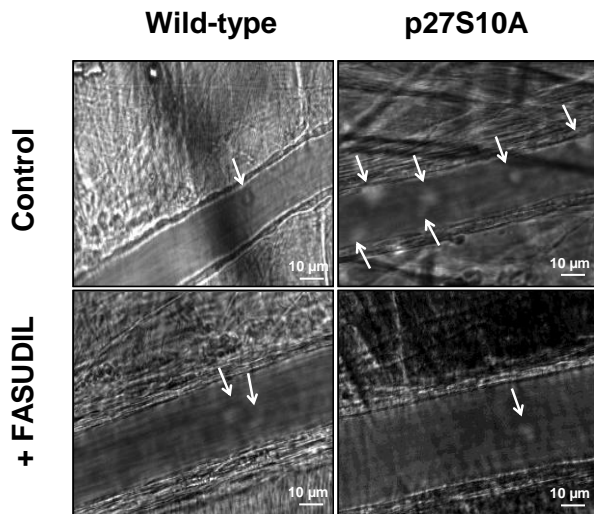


**B**

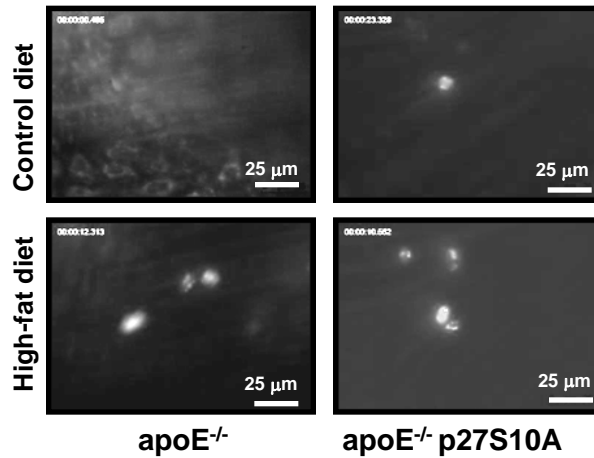
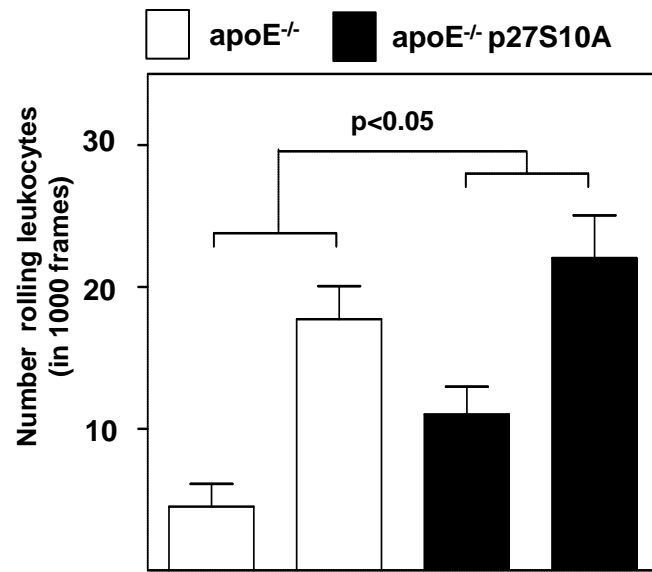


□ Wild-type

■ p27S10A



### A Intravital microscopy carotid artery



### B Leukocyte homing into aorta (adoptive transfer)

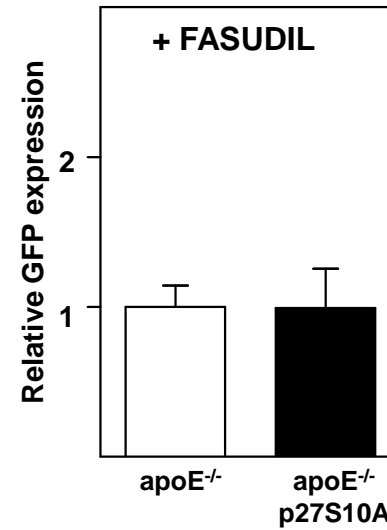
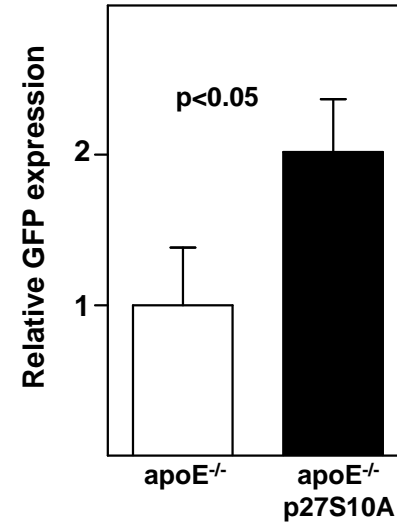
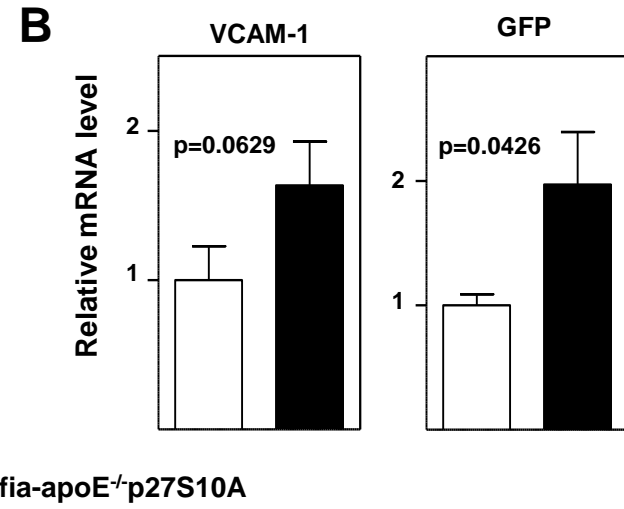
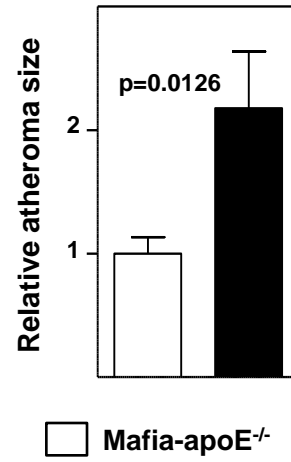
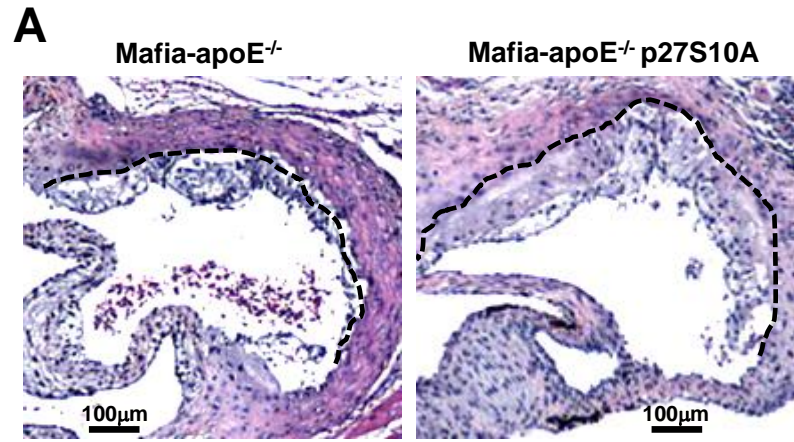


Figure 6

Figure 6



+ FASUDIL

